Environmental Microbiology (2008) **10**(9), 2344–2354 doi:10.1111/j.1462-2920.2008.01660.x

Measurements of accumulation and displacement at the single cell cluster level in *Pseudomonas aeruginosa* biofilms

Benjamin J. Klayman,[1] Isaac Klapper,[1,2] Philip S. Stewart[1,3†] and Anne K. Camper[1,4*]
[1]*Center for Biofilm Engineering, 366 EPS Building, Montana State University, Bozeman, MT 59717, USA.*
[2]*Department of Mathematical Sciences, Wilson Hall, Montana State University, Bozeman, MT 59717, USA.*
[3]*Department of Chemical and Biological Engineering, 301 Cobleigh Hall, Montana State University, Bozeman, MT 59717, USA.*
[4]*Department of Civil Engineering, 201 Cobleigh Hall, Montana State University, Bozeman, MT 59717, USA.*

Summary

Quantitative descriptions of biofilm growth and dynamics at the individual cell level are largely missing from the literature. To fill this gap, research was done to describe growth, accumulation and displacement patterns in developing *Pseudomonas aeruginosa* biofilms. A parent strain of PAO1 was labelled with either a cyan or yellow fluorescent protein. These were then grown in a flow cell biofilm together so that pockets of dividing cells could be identified and their accumulation and displacement tracked. This analysis revealed a pattern of exponential accumulation for all clusters followed by a stationary accumulation phase. A background 'carpet' layer of cells uniformly colonizing the surface exhibited zero net accumulation of bio-volume. The individual clusters were found to have a mean accumulation rate of 0.34 h^{-1} with a range of 0.28–0.41 h^{-1}. Cluster accumulation rates were negatively correlated with cluster size; larger clusters accumulated volume at a slower rate ($P < 0.001$). Pockets of cells on the inside of clusters initially accumulated at a comparable rate to the cluster within which they resided, but later invariably exhibited zero to slightly negative accumulation despite continued exponential (positive) accumulation of the cluster. Expanding clusters were able to displace neighbouring cells from the surface, and larger clusters displaced smaller clusters. This work provides a more detailed quantitative experimental observation of biofilm behaviour than has been described previously.

Received 20 July, 2007; accepted 13 April, 2008. *For correspondence. E-mail anne_c@erc.montana.edu; Tel. (+1) 406 994 4906; Fax (+1) 406 994 6098. †Correction added on 27 June, after first online publication: the third author's name was corrected from Phillip Stewart to Philip Stewart.

Introduction

The relationship between biofilm structure and biofilm activity has been well established in glass flow cells using confocal microscopy and image analysis tools. Klausen and colleagues (2003a) described cluster development occurring primarily as a function of clonal growth. Seeding dispersal from the inside-out of clusters larger than 80 μm in diameter (40 μm radius) resulted in hollow clusters (Purevdorj-Gage *et al*., 2005). Interior regions of biofilm clusters have previously been shown to be nutrient-limited both experimentally (DeBeer *et al*., 1994; Werner *et al*., 2004) and in mathematical models (Wanner and Gujer, 1986; Picioreanu *et al*., 1998; Dockery and Klapper, 2001; Roberts and Stewart, 2004). Under the conditions studied, nutrient limitation was observed to occur at an approximate depth of 40–50 μm. Measurements of metabolic activity have likewise shown these regions to be less active (Sternberg *et al*., 1999; Walters *et al*., 2003; Werner *et al*., 2004; Rani *et al*., 2007). Fluorescent stains have been used to measure activity, including acridine orange for overall physiological activity (Moller *et al*., 1995), and BrdU and an inducible GFP construct to study DNA and protein synthetic activity in staphylococcal biofilms (Rani *et al*., 2007).

Quantitative image analysis of confocal scanning laser microscopy images of developing biofilms has revealed strong correlations between biofilm structure and biofilm processes (Beyenal *et al*., 2004a). Image analysis techniques have evolved from initial measurements of thickness variability and roughness (Stewart *et al*., 1993; Murga *et al*., 1995), to extensive Matlab (The MathWorks) scripts for calculating various biofilm-relevant parameters. Such programs include ISA (Yang *et al*., 2000; Beyenal *et al*., 2004b), COMSTAT (Heydorn *et al*., 2000) and the more recently developed PHLIP (Mueller *et al*., 2006). These programs report on 'averaged' values for multiple clusters within a field of view, and have largely ignored descriptions at the single cluster level.

© 2008 The Authors
Journal compilation © 2008 Society for Applied Microbiology and Blackwell Publishing Ltd

Biofilm modelling has become an important tool for investigating biofilm phenomena. Current biofilm models are being evaluated against experimentally obtained data, which is an important advancement. However, these comparisons are still largely qualitative, exemplified by Picioreanu and colleagues (2007) who evaluate their results as 'in good qualitative agreement with the experimental data'. While macro-scaled, averaged information is useful, more quantitative experimental data at the individual cell/cell cluster level is needed to aid in careful model validation. These models rely on a set of rules which govern the behaviour of individual bacterial cells, but these rules have largely not been validated with experimental observations at the single cell level. For example, cells in cellular automata models are left to move to randomly generated locations at arbitrary velocities (Hunt *et al*., 2003).

Attempts have been made to quantify the movement of cells in biofilms, but the information is limited. Initial events have been previously characterized (Rice *et al*., 2000; 2003) where it was shown that cells that initially attach to a surface undergo a lag phase prior to growth. The displacement velocity of cells growing in young (3–10 μm thick) biofilms was measured to be 1.0 μm h^{-1}. These experiments were limited by the use of only a single fluorescent label and, therefore, the behaviour of individual cells within a biofilm cluster could not be discerned. Because of advances in fluorescent protein technology, bleed-over free detection of two fluorescent labels simultaneously within a biofilm community is now possible (Bloemberg *et al*., 2000; Kjaergaard *et al*., 2000; Klausen *et al*. 2003a,b; Lequette and Greenberg, 2005). This advancement now allows for quantitative information to be obtained on the behaviour of neighbouring cells within complex biofilms.

This work examined developing biofilm clusters and their interactions with neighbouring cells and cell clusters during the rapid (exponential) accumulation phase. Quantification was achieved manually, giving the user freedom to extract information from individual clusters or pockets of dividing cells within clusters. Bio-volumes were calculated for the entire field of view, individual clusters within a field of view and small pockets of cells within single clusters. In addition to accumulation, centroid locations were measured at the individual cell level, resulting in localized displacement vectors for individual cell pockets within clusters.

Results

Behaviour of labelled subpopulations

The cyan and yellow subpopulations were grown separately in batch culture and their ln-transformed cell counts plotted against time. A least-squares line was then fit to the linear portion of the plot (2–8 h) and the slope of the line reported as the maximum specific growth rate, μ_{max}. The mean (± SEM) maximum specific growth rates were 0.32 (± 0.04) and 0.36 (± 0.05) h^{-1} for cyan and yellow respectively. The difference in growth rates was not statistically significant ($P = 0.57$).

The yellow and cyan subpopulations were grown separately in flow cells to compare the bio-volumes of the biofilms. The two biofilms were visually similar, with a carpet of cells uniformly colonizing the surface punctuated by large, isolated clusters growing from the carpet (data not shown). When grown together, the pattern of growth was identical, with a carpet of cells punctuated by isolated clusters, some yellow and some cyan. However, the carpet consisted primarily of yellow cells, with only a few cyan cells dispersed throughout. Effluent was collected at the end of each dual label experiment and drop plated to obtain viable plate counts for each label. Slightly more cyan cells were detected in the effluent ($P = 0.015$) with the average plate counts 3.6×10^6 and 5.1×10^6 for yellow and cyan respectively. The effluent from the flow cell was plated on Tryptic Soy Agar (TSA, BD Difco; http://www.fishersci.com) with and without antibiotic to check for loss of plasmid. There was no significant difference between the antibiotic and non-antibiotic plate counts ($P = 0.14$).

Accumulation of individual cell clusters

Figure 1 shows confocal images of a growing biofilm composed of both cyan and yellow cells as seen from the bulk fluid (top panel), through the glass (middle panel) and a recreation made with the yellow channel only (bottom panel, 1A only). Clusters comprised predominantly of a single label (either cyan or yellow) arose from the carpet of cells. Both cyan and yellow bacteria carpeted the individually grown flow cells, but yellow bacteria dominated the mixed flow cell carpet layer. As seen in the view through the glass (middle panel), the large cluster in the centre has hollowed out dramatically, with little to no hollowing observed in the other, smaller clusters. From transmitted light images, it was clear that the internal area was void of cells, as opposed to containing cells which had lost their fluorescence (data not shown). Additionally, the group of clusters to the above right of the main cluster expanded to form one undifferentiated cell cluster, having displaced the yellow cells that originally were on the glass between the cyan clusters. From the portrayal with the yellow only (bottom panel, 1A), the main cluster is displacing cells on the surface as it expands with the displaced cells accumulating on the edge of the expanding cluster. Three easily recognizable yellow pockets of cells were located within the cyan cluster. Movies of these time-lapse

© 2008 The Authors
Journal compilation © 2008 Society for Applied Microbiology and Blackwell Publishing Ltd,

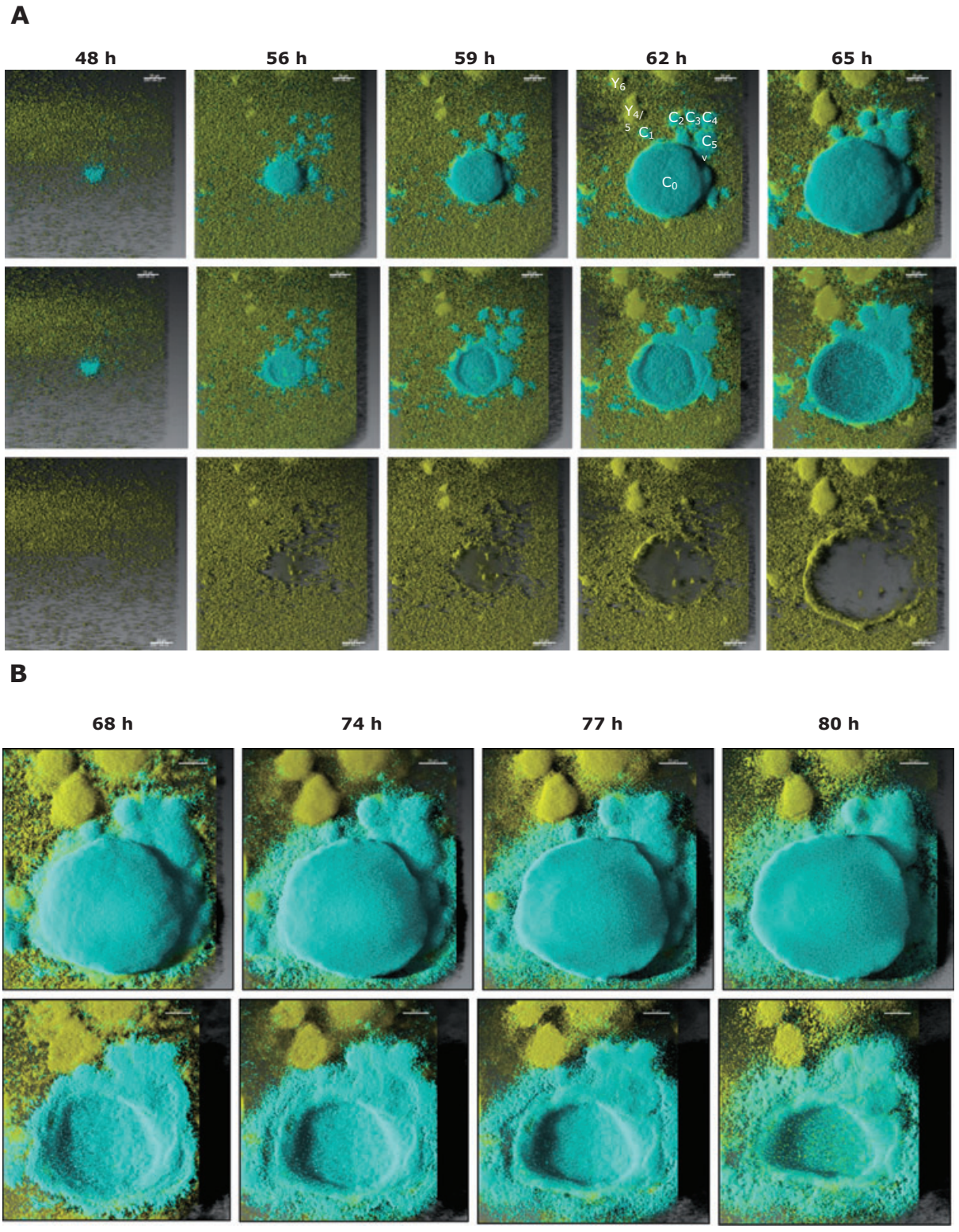

Fig. 1. A. Time-lapse confocal images showing exponential accumulation of *P. aeruginosa* biofilm in a capillary flow cell. Viewed from the bulk fluid (top panel), individual clusters are seen rising from the background carpet of cells. The same series viewed through the glass (middle panel) reveals that the large cyan cluster was hollowed out. Viewed without the cyan (bottom panel), it is clear that the expanding cluster displaces the neighbouring carpet cells, which accumulate on the side of the cluster.
B. Stationary phase of biofilm accumulation. At 80 h, yellow cells appear inside of the cluster, indicating that cells from the bulk fluid are penetrating inside the cluster.

© 2008 The Authors
Journal compilation © 2008 Society for Applied Microbiology and Blackwell Publishing Ltd,

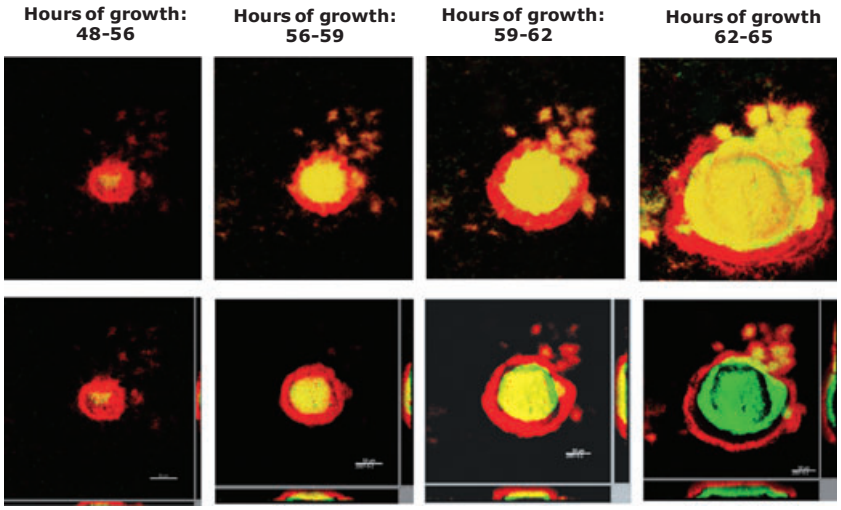

Fig. 2. Overlays of successive time points in maximum projection (top panel) or cross section (bottom panel) during exponential accumulation. In all images, the earlier time point is labelled green, and the later point red. As such, in the overlay images green would indicate biomass which migrated during the interval, red indicates new biomass and yellow indicates biomass that was present at both the old and new time points.

representations can be seen on the CBE website at (http://www.biofilm.montana.edu/Res-Lib99-SW/Movies/Database/MD_DisplayScript.asp).

Additional information about where in the cluster accumulation was occurring could be obtained by overlaying successive time images of the same field of view. These are shown in a top view maximum projection (top panel) and in cross section (bottom panel) in Fig. 2. From the maximum projection depiction, it is seen that new growth (indicated with false colour red) occurred uniformly around the large cluster (centre of image) at the earlier time points (48–59 h) and was seen to preferentially accumulate biomass on the lower side of the cluster at the later time points (59–65 h). This shift in accumulation pattern coincided with the large cluster coming into physical contact with the smaller group of clusters at the upper right.

Additional information regarding outward spreading versus upward spreading was obtained by looking closer at the cross sections (Fig. 3). One way to examine this is to compare the accumulation of cells in microns upwards (increase in maximum height) and outwards (increase in cluster radius). During the intervals 56–59, 59–62 and 62–65 h, the accumulation of cells resulted in a net radius increase of 22, 23 and 23 μm respectively, versus a net increase in maximum height of 10, 12 and 32 microns. Or, upward accumulation was 45%, 52% and 139% of outward accumulation. The cluster was observed to hollow out during the exponential accumulation phase, with initial hollowing occurring at a cluster diameter of 112 μm (radius 56 μm). A dramatic increase in hollowing occurred between 62 and 65 h of growth, coinciding with the largest increase in maximum height.

A plot of the natural log of the volumes versus time for each individual cluster as labelled on Fig. 1 is shown in Fig. 4. From 48 to 65 h, the individual clusters exponentially accumulated volume and exhibited a mean accumulation rate (λ_b) of 0.34 ± 0.04 h^{-1} with r^2 values greater than or equal to 0.98. In addition to the clusters, the accumulation of the carpet region of cells inside of an arbitrarily drawn 50 μm × 50 μm box was calculated and was not significantly different from zero ($P = 0.06$).

Accumulation rates for individual clusters were plotted against cluster size to check for a correlation (Fig. 5). Accumulation rate was found to decrease significantly as cluster size increased ($r = -0.64$, $P < 0.001$).

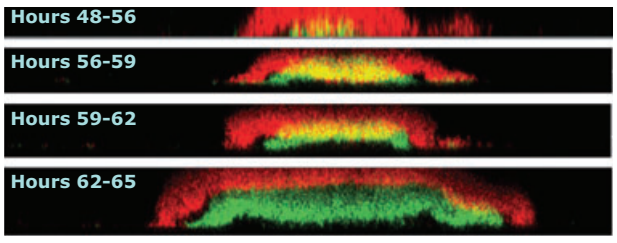

Fig. 3. Cross-section overlays during exponential accumulation. Hollowing begins to occur in a ring near the edges, as indicated by green in the second and third panels. Cluster was seen to dramatically hollow out (bottom panel) despite remaining in exponential accumulation phase.

Displacement of individual cell clusters

To measure the variability in the method of centroid calculation described in this research, the centroid coordinates of five clusters were calculated three successive times. The standard deviations of the measurements of 0.01–0.24 μm were between two and four orders of magnitude smaller than the mean displacement being measured.

The centroids (x, y coordinates) of all objects projected onto the xy plane were measured and used to calculate displacement directions and velocities (Table S1). Clusters which had no encroaching neighbouring clusters had

© 2008 The Authors
Journal compilation © 2008 Society for Applied Microbiology and Blackwell Publishing Ltd,

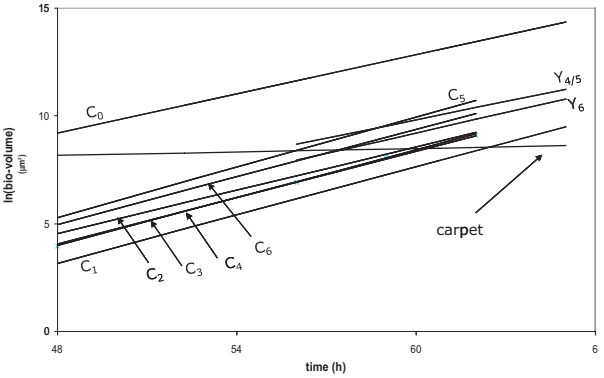

Fig. 4. Exponential phase of accumulation for all identifiable clusters shown in Fig. 1. The clusters are all accumulating at approximately the same rate (mean 0.34 h^{-1}), except for the carpet which was not significantly accumulating with time.

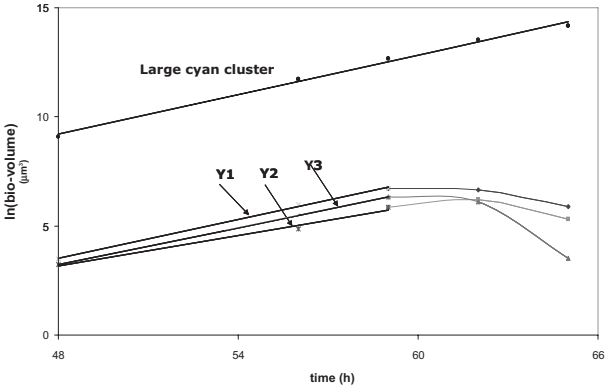

Fig. 6. Accumulation of three small yellow pockets of cells contained inside of the large cyan cluster shown in Fig. 1. Pocket accumulation was exponential from 48 to 59 h, and which time accumulation stopped and some loss of volume occurred.

the least displacement (C1, C2, Y4, Y5) with total displacements ranging from 1 to 5 μm, corresponding to velocities between 0.1 and 1 μm h^{-1}. Clusters that came into physical contact with neighbouring clusters (C0, C8) exhibited larger displacements which were along the line made by connecting the two centroids. Total displacements for these clusters ranged from 10 to 42 μm, corresponding to velocities between 3 and 7 μm h^{-1}. The individual cells of the carpet neighbouring the large cyan cluster were displaced 97 μm from their original position, corresponding to a maximal velocity of 10 μm h^{-1}.

Pockets of cells within clusters

Pockets of cells were defined as a group of cells of one fluorescent label inside of a cluster comprised predominantly of the other label. A more detailed analysis was performed on the three pockets of yellow cells contained within the large cyan cluster. The natural logs of their volumes are plotted versus time in Fig. 6. An analysis of their accumulation rates between 48 and 59 h revealed that they were accumulating at approximately 90% of the rate for the overall cluster. Between 59 and 65 h, however, the pockets of yellow cells inside stopped accumulating bio-volume, even exhibiting a net loss, while the large cluster continued accumulating exponentially.

As these pockets were not attached to the substratum, the z coordinate of the centroid was calculated and used to further understand accumulation and displacement at three-dimensional localized regions inside growing biofilm clusters. The volume, maximum height, maximum width, centroid (z coordinate) and 3D total displacement velocity are reported in Table S2. Pockets Y2 and Y3 expanded more in the z direction relative to the xy plane than Y1 and exhibited the lowest accumulation rates. Pocket Y1 was seen to accumulate volume almost exclusively in the xy plane, and exhibited the highest accumulation rate. Between hours 62 and 65, when the overall cluster maximum height increased from 56 to 89 microns (the largest incremental increase), the centroids of the small pockets were likewise seen to dramatically increase in z position despite a decrease in volume. When factoring in changes in the z coordinate of the centroid, the small pockets exhibited a maximum displacement velocity of 9.6 μm h^{-1}. The xy displacement for Y1 and Y2 was highly correlated with their radial location within the cluster.

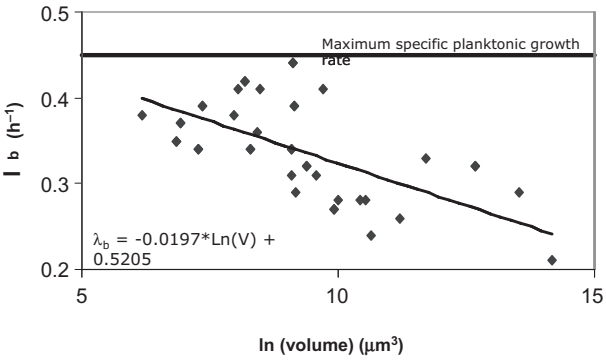

Fig. 5. Relationship between cluster volume and accumulation rate (λ_b). Accumulation rate appears upper bound by the planktonic growth rate.

Stationary accumulation phase

After the period of exponential accumulation, the biofilm exhibited a stationary or quasi-steady state phase (hours 65–80). Cluster volume is plotted against time for the entire 32 h experiment in Fig. 7. In this stationary phase, bio-volume was decreasing slightly, although not significantly different from zero ($P = 0.21$). Figure 1B shows the corresponding images as viewed from the bulk fluid (top panel) and through the glass substratum (bottom panel).

© 2008 The Authors
Journal compilation © 2008 Society for Applied Microbiology and Blackwell Publishing Ltd,

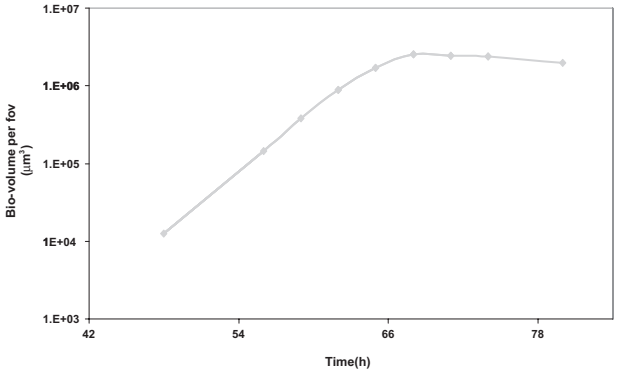

Fig. 7. Overall accumulation for the entire field of view (cyan only) shown in Fig. 1. An exponential accumulation phase (hours 48–65) was followed by a stationary accumulation phase (hours 68–80).

From the bulk fluid, it appears that the structure of the large cyan cluster was not changing. However, when viewed through the glass, it is clear that the outer shell was 'retracting' inwards at the site of attachment to the glass, resulting in a decrease in diameter. This is shown in cross section in Fig. 8. From this view, it can be seen that retraction occurred primarily where the greatest initial displacement occurred, namely the lower edge. The cluster remained a hollow shell, decreasing in attached diameter at the same time as increasing in maximum height until reaching 140 μm at 77 h. A break was seen in the shell beginning at 65 h and, by 80 h, the cluster was invaded by yellow planktonic cells (Fig. 1B, bottom panel).

Overall patterns

This experiment was repeated to verify patterns of accumulation and displacement. This experiment revealed repeatable accumulation and displacement patterns. Individual clusters of predominantly one label were observed to rise from a background carpet of cells (Fig. 9). Individual clusters accumulated exponentially with a mean accumulation rate of 0.37 ($\pm$ 0.04) h^{-1}. As previously, the accumulation of cells in the background carpet was low ($\lambda_b = 0.05$), although a linear regression verified that the value was significantly different from zero ($P = 0.025$). Three clusters that had no encroaching neighbours displaced less than 3 μm. A pocket of cyan cells near the centre of the large yellow cluster was displaced 8 μm over the course of the experiment, compared with a pocket of cells near the edge which displaced 20 μm. The pocket near the centre was seen to initially accumulate at the rate of the larger cluster. When the larger cluster radius reached 50 μm, the pocket of cells stopped accumulating while the larger cluster continuing exponential expansion.

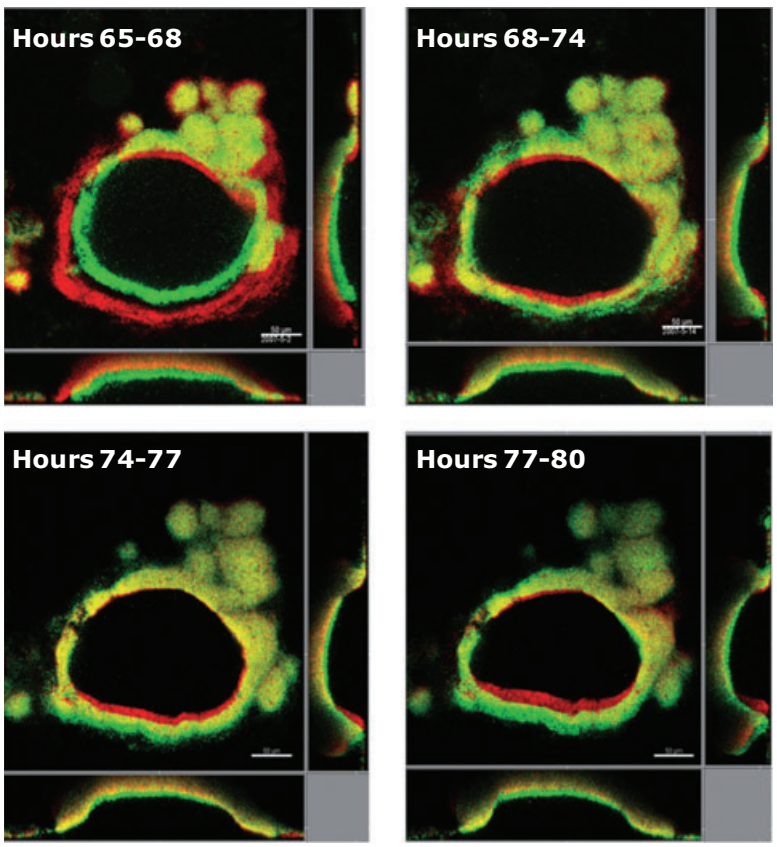

Fig. 8. Successive time overlay cross sections during stationary phase of biofilm accumulation. Plan view image approximately 10 μm from the glass substratum. Cluster expands outward (some accumulation occurs hours 65–68), then is followed by a period of continued upward expansion but inward retraction (no accumulation, hours 68–80). A break is seen forming on the left side of the cluster beginning at hour 65.

© 2008 The Authors
Journal compilation © 2008 Society for Applied Microbiology and Blackwell Publishing Ltd,

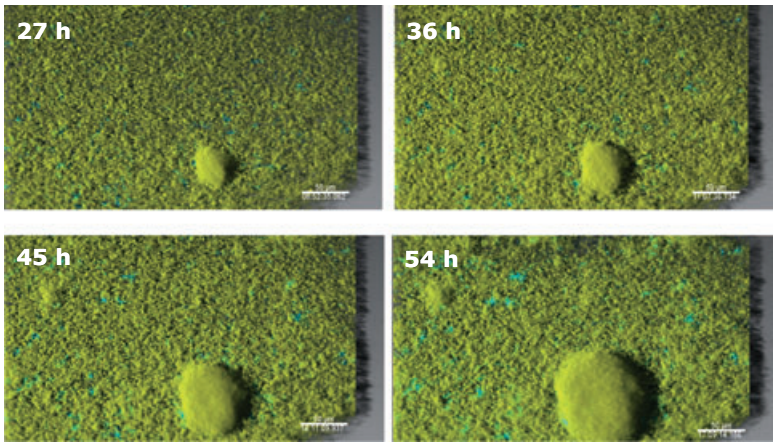

Fig. 9. Time-lapse confocal images showing repeatable biofilm formation pattern observed in flow cell. The large cluster is comprised predominantly of yellow cells, with small pockets of cyan cells in the centre and near the edges.

Discussion

Every effort was made to ensure that the two labelled subpopulations used in the present study were identical. The two plasmids were identical except for the fluorescent gene insert and were inserted into the same parent strain. Despite these precautions, some differences were observed. The yellow cells grew slightly faster in batch culture (0.36 versus 0.32 h^{-1}), although this difference was not statistically significant. Despite this, there were more cyan cells detected in the effluent from the mixed-labelled biofilm ($P = 0.015$). As the parent strain and the plasmid were identical in both labelled subpopulations, this difference in behaviour must be due to some burden unique to the fluorescent protein. This difference warrants further investigation, as many researchers are using dual-labelled subpopulations for bacterial biofilm study.

An analysis of the accumulation rates of individual clusters shown in Fig. 1 revealed a mean accumulation rate of 0.34 h^{-1}. The measured accumulation rate for cluster volumes is a function of cell growth and detachment. The theoretical maximum accumulation rate should then be bounded by the planktonic growth rate (maximum growth, detachment = 0). Because the accumulation rate is near maximum growth rate (0.36 h^{-1}), this suggests that the effects of detachment are relatively minor and that the effect of substrate limitation is limited.

As the clusters reached stationary phase, the retarded accumulation rate could be attributed either to slowed growth of the cluster, presumably as a result of nutrient limitation, or increased detachment. Lower metabolic activity has previously been measured in the interior regions of larger biofilm clusters (Sternberg *et al*., 1999; Walters *et al*., 2003; Werner *et al*., 2004; Rani *et al*., 2007) which would result in retarded accumulation rates for larger clusters. In the present study, accumulation rate was negatively correlated with cluster size. The three yellow pockets in the interior of the large cyan cluster accumulated at a slightly lower rate (90%) compared with the overall cluster, suggesting that slower growth is occurring in the interior regions of the biofilm. Additionally, the cluster became hollow and the three pockets of yellow cells in the interior region of the cluster decreased in volume and eventually eroded completely, suggesting that detachment contributed to the phenomenon.

The phenotype of clusters forming dense 'walls' or 'shells' with hollow interiors has been observed and reported previously and was shown to be quorum sensing-dependent (Purevdorj-Gage *et al*., 2005). In this previous study, biofilms differentiated into the hollowed phenotype at a cluster radius of 40 μm, slightly smaller than the 55 μm observed here. This is not surprising, as both the nutrient conditions and flow rate were different which have both been shown to affect biofilm structure (Dunsmore *et al*., 2002; Klausen *et al*., 2003b). In both studies, the cluster wall thickness remained constant despite changes in void area. In the present study, the 'wall' initially migrated outward in only one direction (downward, Fig. 2) followed by a retraction at that same edge (Fig. 8).

A three-dimensional analysis of the displacement of individual yellow pockets of cells inside the larger cyan cluster helps elucidate the mechanism by which the cluster hollows. All three yellow pockets of cells at 62 h were located entirely at a position corresponding to a location absent of cells (hollow) at 65 h. If hollowing occurred solely by dispersion, the pockets of cells should have dispersed; rather, the same pockets of cells were still present, but at a much higher z coordinate. This behaviour suggests that the cluster is 'inflating' like a balloon rather than hollowing occurring solely by cells dispersing (detaching) from the inside. The yellow pockets did lose significant volume during this time period, suggesting that the process may occur through a combination of both erosion and inflation.

© 2008 The Authors
Journal compilation © 2008 Society for Applied Microbiology and Blackwell Publishing Ltd,

Much attention in the literature has been directed at details of growth of biofilm structures. In contrast, effects and influences of material properties and mechanics in biofilm development have been relatively neglected. The present study suggests that such factors may be important and require further study. As a particular example, inflation at the cluster top and contraction at the cluster bottom following hollowing are suggestive of mechanical relaxation as a result of dispersion of interior cells and matrix. Additionally, displacement direction of individual smaller clusters in the fields of view observed was found to be independent of fluid flow direction, but was similar to the angle of neighbouring clusters that came into contact with displaced clusters. Indeed, the fact that biofilm morphology is not obviously dependent on fluid flow direction suggests that cohesive forces are important at least in this system.

The accumulation rates for the carpet areas in the two studies reported here were 0.02 and 0.05 h^{-1}, and in the first study were not significantly different from zero. An examination of the centroid coordinates for individual cells in the carpet that were not immediately adjacent to a cluster revealed little displacement (data not shown) in this laminar flow system. This suggests that the cells are likely not growing as rapidly, rather than growing and detaching, to account for the low accumulation rate as compared with biofilm clusters (mean 0.34 h^{-1}). This kind of self-generated diversity may be common and important in biofilms (Boles *et al*., 2004) and has generally been neglected in modelling efforts. Significant displacement occurred for cells in the carpet adjacent to exponentially accumulating clusters as well as smaller clusters adjacent to larger clusters. This is highly suggestive of mechanical forces being the dominant mechanism for displacement transport. The carpet of cells at the lower edge of the large cyan cluster displaced 97 μm on the projected xy plane over the 32 h experiment, corresponding to a maximum velocity of 10 μm h^{-1}. In contrast, Rice and colleagues (2003) noted displacement velocities of only 1 μm h^{-1} in young (3–10 μm thick) biofilms.

Information about localized velocities within biofilms is very important. Much of the biofilm modelling effort has focused on effects of growth on biofilm morphology (Wanner and Gujer, 1986; Picioreanu *et al*., 1998; Dockery and Klapper, 2001; Cogan and Keener, 2004). A key observation of these models is that the distribution pattern of growth (and the resulting growth-induced local velocity field) may have an important influence on biofilm heterogeneity. Furthermore, modellers have recently begun considering the effects of other mechanical processes, such as visco-elasticity, cohesion and shear stress, on biofilm geometry (Xavier *et al*., 2005; Klapper and Dockery, 2006). All of these effects also produce identifiable signatures in local, internal velocity fields. Hence, the observations of local velocity are of great interest in that they help identify the relative importance of different mechanical processes present in biofilms.

Displacement direction of individual cell pockets in the present study was along their radial coordinates. Radial displacement is consistent with model predictions of growth-based biofilm velocities (Dockery and Klapper, 2001; Cogan and Keener, 2004). The fact that a large cluster displaces surrounding carpet cells rather than engulfing them would seem to suggest that cohesive energy is important, i.e. cluster cells prefer adhering to themselves over carpet cells. Such 'extra-cohesivity' may be an important component of cluster formation, distinguishing cluster-forming cells from carpet-forming ones.

Experimental procedures

Bacterial strains, plasmids and media

Pseudomonas aeruginosa PAO1 was used for all experiments. The parent population (CBE archive) was tagged with plasmid-borne cyan fluorescent protein (CFP) or yellow fluorescent protein (YFP). The two plasmids (pUCP22Not) contained a carbenicillin-resistance gene and were identical except for the fluorescent protein gene insert. The plasmids were obtained from Morten Hentzer at the Technical University of Denmark. The PAO1 cells were made competent by taking 1 ml of an overnight culture grown in Luria–Broth (LB, Difco) and spiking it into 200 ml fresh LB broth and shaking for 2 h at 30°C. This culture was then spun down successively three times and finally re-suspended in 500 μl of cold, sterile 10% glycerol. The plasmids were then inserted by electroporation (Eppendorf Electroporator 2510; 1500 V) and the cells plated on Pseudomonas Isolation Agar (Difco) + 250 mg l^{-1} carbenicillin (Fisher Bioreagents). All planktonic and biofilm experiments were conducted using 10% Tryptic Soy Broth (TSB, EMD; http://www.emdchemicals.com) + 250 mg l^{-1} carbenicillin.

Planktonic growth curves

Cells were streaked for isolation from a frozen glycerol stock on TSA. A single colony was placed into 4 ml of 10% TSB and shaken 24 h at 180 r.p.m. at 25°C. 1.5 ml of this culture was then spiked into 150 ml of fresh 10% TSB and shaken at 180 r.p.m. at 25°C. This flask was then used for the growth curve. At each sample time, 500 μl was serially diluted (1/4× Ringer, Oxoid) and plated using the drop plate method (Herigstad *et al*., 2001) for viable cell counts. μ_{max} values are reported as the mean (±SEM) for six replicate trials and were calculated by obtaining the slope of the least-squares fitted line of the ln (cfu ml^{-1}) versus time plot during exponential phase (hours 2–8.5).

© 2008 The Authors
Journal compilation © 2008 Society for Applied Microbiology and Blackwell Publishing Ltd,

Biofilm reactor design and operation

Biofilms were grown in 0.9 mm inside diameter glass capillary tubes (Friedrich and Dimmock, http://www.fdglass.com). The glass tubes (baked at 300°C, 5 h) have a square cross section, allowing direct microscopic observation of biofilm colonizing the inside of the tube through the flat tube wall. The flow cell was fed by silicone tubing with an inoculation port 10 cm upstream from the flow cell. The assembly was autoclaved 20 min prior to inoculation. Inoculum cultures were prepared by first streaking for isolation on TSA + 250 mg l^{-1} carbenicillin. A single colony was placed into 4 ml of 10% TSB + 250 mg l^{-1} carbenicillin and shaken overnight at 30°C. 1.5 ml of the overnight culture was then spiked into 150 ml of fresh TSB + 250 mg l^{-1} carbenicillin and shaken at 30°C for 5 h. These cultures were then inoculated individually for single labelled biofilms, or mixed in a 50/50 volumetric ratio and vortexed for 5 s for mixed biofilms, and inoculated into the flow cell using a 1 ml syringe. In all cases, the cells were allowed a 3 h static attachment period, at which point flow of sterile 10% TSB + 250 mg l^{-1} carbenicillin was resumed. Biofilm was allowed to form for 36–48 h before the flow cell was brought to the microscope for observation. Downstream of the flow cell was a port which was open for collecting effluent samples, and closed for normal operation. Design flow rate was 24 ml h^{-1} which corresponds to a Reynolds number of 10 predicting laminar flow conditions. All biofilm experiments were carried out at 25 ± 2°C.

Confocal microscopy

All images were taken on a Leica SPS2 AOBS single photon confocal microscope equipped with 458 laser set to 75% power for CFP excitation and a 496 nm laser set to 20% power for YFP excitation to minimize cross-over effects. PMT values were set at the beginning of the experiment and remained fixed for the duration of the experiment. PMT1 (CFP) was set at 525 and PMT2 (YFP) set to 475, with the pinhole set to 1.0. Three-dimensional stacks were collected at 3 h intervals at a single field of view. One 10× (HC PL Fluotar 0.3 NA, Dry) and one 40× (HCX APO U-V-I 0.8 NA, Water) image were collected at each time point so that only the objective (not the stage) was moved. The Imaris software package (Bitplane AG, Zurich Switzerland) was used to recreate confocal images into three-dimensional renderings.

Accumulation rate calculations

All quantitative analysis of the data was performed using Metamorph (Version 7.0, Molecular Devices). The threshold value was set manually for each fluorescent label (cyan or yellow), then applied uniformly to all images. The pixels (calibrated to μm) with an intensity value above the threshold value in each plane were counted by Metamorph using the Region Measurements function, converted to area (μm^2), exported into Microsoft Excel and summed over the set of z-stack planes. Bio-volumes were obtained by multiplying the sum of the calculated areas by the distance between planes resulting in bio-volume (μm^3) for each species. As only the pixels with an intensity greater than the threshold value were counted, hollow regions of clusters were not included in the bio-volume measurement.

User-defined script was written in the Metamorph software for calculating bio-volumes of each subpopulation. The user-defined script allowed for volume calculation at any location within the reactor, so that wherever a cluster or pocket of cells was identifiable from its neighbours, its volume was calculated. For the purposes of the present study, a pocket of cells refers to a group of cells of one label inside of a cluster predominantly comprised of cells of the other label. The specific accumulation rate was based on a first-order kinetic model and was defined as $\lambda_b = \frac{\ln\left(\frac{V_2}{V_1}\right)}{t_2 - t_1}$, where λ_b = biofilm (volume) accumulation rate (h^{-1}), and V_2 and V_1 correspond to the calculated bio-volumes (μm^3) at times t_2 and t_1 (h) respectively. As localized detachment could not be measured, this value represents the combined effects of growth and detachment. This value was calculated in the same manner as the planktonic maximum-specific growth rate; that is, by plotting ln (V) versus time during exponential accumulation, and finding the slope of the least-squares regression line.

Displacement calculations

The position of the centroid was monitored over time for each cluster or pocket of cells within a cluster. The same threshold value was used as for the accumulation rate calculations. The maximum projection onto the xy plane of a z stack of images was created in Metamorph. Objects were traced in Metamorph using the Trace Objects function, then the Shrink to Fit function was applied to the traced region to exactly trace the outline of a thresholded cluster or pocket of cells. The centroid of the traced region was then measured using the Integrated Morphometry Analysis feature and the *x*, y coordinates of the centroid were exported to Microsoft Excel. The z coordinate of the centroid was calculated by finding the z plane which corresponded to the midpoint of accumulated volume. Velocities were obtained by dividing the change in distance by the change in time for two successive centroid measurements of the same object. Displacement velocities are referenced in two ways: (i) v_{xyz}, the total velocity (μm h^{-1}) by using the total change in Euclidian distance per h and (ii) v_{xy}, the horizontal velocity (μm h^{-1}) on the projected xy plane by using only the change in x and y direction. Net displacement was defined and measured as the distance between the final centroid position of an object and its initial position. The displacement angle (θ) between centroids was calculated on the xy projections relative to horizontal, such that θ varies between zero (downstream) and 360° increasing in the counter-clockwise direction.

To address the variability in the method of centroid calculations, objects were traced and the centroids calculated. The images were then closed, re-opened, and the objects traced again. This was performed three times. The standard deviations were then calculated for each traced object as a measure of variability.

Effluent analysis

A minimum of 500 μl of effluent was collected at the end of each experiment, disaggregated by vortexing for 20 s,

© 2008 The Authors
Journal compilation © 2008 Society for Applied Microbiology and Blackwell Publishing Ltd,

serially diluted (1/4× Ringer) and plated on TSA and TSA + 250 mg l^{-1} carbenicillin plates for viable plate count analysis. The plates were then re-counted on a Nikon epifluorescent microscope (10×, HC PL Fluotar 0.3 NA, Dry) with filters for CFP and YFP and the colony counts of each respective subpopulation recorded.

Statistical analysis

Statistical analysis was performed using Minitab Release 14. Unless otherwise noted, a *t*-test was used to test for statistically significant differences between means. *P*-values smaller than 0.05 were considered significant.

Acknowledgements

This research has been supported by the Keck Foundation and a grant (DAAD 19-03-1-0198) from the Army Research Office. Any opinions, findings and conclusions or recommendations expressed in this material are those of the authors and do not necessarily reflect the views of the Army Research Office. The confocal microscope was provided via support from the Murdock Charitable Trust. The authors also gratefully thank Dr Martin Hamilton for his statistical assistance.

References

Beyenal, H., Lewandowski, Z., and Harkin, G. (2004a) Quantifying biofilm structure: facts and fiction. *Biofouling* **20:** 1–23.

Beyenal, H., Donovan, C., Lewandowski, Z., and Harkin, G. (2004b) Three-dimensional biofilm structure quantification. *J Microbiol Methods* **59:** 395–413.

Bloemberg, G.V., Wijfjes, A.H., Lamers, G.E., Stuurman, N., and Lugtenberg, B.J. (2000) Simultaneous imaging of *Pseudomonas fluorescens* WCS365 populations expressing three different autofluorescent proteins in the rhizosphere: new perspectives for studying microbial communities. *Mol Plant Microbe Interact* **13:** 1170–1176.

Boles, B.R., Thoendel, M., and Singh, P.K. (2004) Self-generated diversity produces 'insurance effects' in biofilm communities. *Proc Natl Acad Sci* **101:** 16630–16635.

Cogan, N., and Keener, J.P. (2004) The role of biofilm matrix in structural development. *Math Med Biol* **21:** 147–166.

DeBeer, D., Srinivasan, R., and Stewart, P.S. (1994) Direct measurement of chlorine penetration into biofilms during disinfection. *Appl Environ Microbiol* **60:** 4339–4344.

Dockery, J., and Klapper, I. (2001) Finger formation in biofilm layers. *SIAM J Appl Math* **62:** 853–869.

Dunsmore, B.C., Jacobsen, A., Hall-Stoodley, L., Bass, C.J., Lappin-Scott, H.M., and Stoodley, P. (2002) The influence of fluid shear on the structure and material properties of sulphate-reducing bacterial biofilms. *J Ind Microbiol Technol* **29:** 347–353.

Herigstad, B., Hamilton, M., and Heersink, J. (2001) How to optimize the drop plate method for enumerating bacteria. *J Microbiol Methods* **44:** 121–129.

Heydorn, A., Nielsen, A.T., Hentzer, M., Sternberg, C., Givskov, M., Ersboll, B.K., and Molin, S. (2000) Quantification of biofilm structures by the novel computer program COMSTAT. *Microbiology UK* **146:** 2395–2407.

Hunt, S.M., Hamilton, M.A., Sears, J.T., Harkin, G., and Reno, J. (2003) A computer investigation of chemically mediated detachment in bacterial biofilms. *Microbiology* **149:** 1155–1163.

Kjaergaard, K., Schembri, M.A., Ramos, C., Molin, S., and Klemm, P. (2000) Antigen 43 facilitates formation of multispecies biofilms. *Environ Microbiol* **2:** 695–702.

Klapper, I., and Dockery, J. (2006) Role of cohesion in material description of biofilms. *Phys Rev E* **74:** 031902.

Klausen, M., Heydorn, A., Ragas, P., Lambertsen, L., Aaes-Jorgensen, Molin, S., and Tolker-Nielsen, T. (2003a) Biofilm formation by *Pseudmonas aeruginosa* wild type, flagella and type IV pili mutants. *Mol Microbiol* **48:** 1511–1524.

Klausen, M., Heydorn, A., Ragas, P., Lambertsen, L., Aaes-Jorgensen, Molin, S., and Tolker-Nielsen, T. (2003b) Biofilm formation by *Pseudmonas aeruginosa* wild type, flagella and type IV pili mutants. *Mol Microbiol* **48:** 1511–1524.

Lequette, Y., and Greenberg, E.P. (2005) Timing and localization of rhamnolipid synthesis gene expression in *Pseudomonas aeruginosa* biofilms. *J Bacteriol* **187:** 37–44.

Moller, S., Kristensen, C.S., Poulsen, L.K., Carstensen, J.M., and Molin, S. (1995) Bacterial growth on surfaces: automated image analysis for quantification of growth rate related parameters. *Appl Environ Microbiol* **61:** 741–748.

Mueller, L.N., de Brouwer, J.F., Almeida, J.S., Stal, L.J., and Xavier, J.B. (2006) Analysis of a marine phototrophic biofilm by confocal laser scanning microscopy using the new image quantification software PHLIP. *BMC Ecol* **6:** 1.

Murga, R., Stewart, P., and Daly, D. (1995) Quantitative analysis of biofilm thickness variability. *Biotechnol Bioeng* **45:** 503–510.

Picioreanu, C., Van Loosdrecht, M.C.M., and Heijnen, J.J. (1998) Mathematical modeling of biofilm structure with a hybrid differential discrete cellular automaton approach. *Biotechnol Bioeng* **58:** 101–116.

Picioreanu, C., Kreft, J.U., Klausen, M., Haagensen, J.A.J., Tolker-Nielsen, T.T., and Molin, S. (2007) Microbial motility involvement in biofilm structure formation – a 3D modeling study. *Water Sci Technol* **55:** 337–343.

Purevdorj-Gage, B., Costerton, W.J., and Stoodley, P. (2005) Phenotypic differentiation and seeding dispersal in non-mucoid and mucoid *Pseudomonas aeruginosa* biofilms. *Microbiology* **151:** 1569–1576.

Rani, S.A., Pitts, B., Beyenal, H., Veluchamy, R.A., Lewandowski, Z., Davison, W.M., *et al.* (2007) Spatial patterns of DNA replication, protein synthesis, and oxygen concentration within bacterial biofilms reveal diverse physiological states. *J Bacteriol* **189:** 4223–4233.

Rice, A.R., Hamilton, M.A., and Camper, A.K. (2000) Apparent surface associated lag time in growth of primary biofilm cells. *Microb Ecol* **40:** 8–15.

Rice, A.R., Hamilton, M.A., and Camper, A.K. (2003) Movement, replication, and emigration rates of individual bacteria in a biofilm. *Microb Ecol* **45:** 163–172.

Roberts, M.E., and Stewart, P.S. (2004) Modeling antibiotic

© 2008 The Authors
Journal compilation © 2008 Society for Applied Microbiology and Blackwell Publishing Ltd,

tolerance in biofilms by accounting for nutrient limitation. *Antimicrob Agents Chemother* **48:** 48–52.

Sternberg, C., Christensen, B.B., Johansen, T., Nielsen, A.T., Andersen, J.B., Giskov, M., and Molin, S. (1999) Distribution of bacterial growth activity in flow-chamber biofilms. *Appl Environ Microbiol* **65:** 4108–4117.

Stewart, P.S., Peyton, B.M., Drury, W.J., and Murga, R. (1993) Quantitative observations of heterogeneities in *Pseudomonas aeruginosa* biofilms. *Appl Environ Microbiol* **59:** 327–329.

Walters, M.C., Roe, F., Bugnicourt, A., Franklin, M.J., and Stewart, P.S. (2003) Contributions of antibiotic penetration, oxygen limitation, and low metabolic activity to the tolerance of *Pseudomonas aeruginosa* biofilms to ciprofloxacin and tobramycin. *Antimicrob Agents Chemother* **47:** 317–323.

Wanner, O., and Gujer, W. (1986) A multispecies biofilm model. *Biotechn Bioeng* **28:** 314–328.

Werner, E., Roe, F., Bugnicourt, A., Franklin, M.J., Heydorn, A., Molin, S., *et al.* (2004) Stratified growth in *Pseudomonas aeruginosa* biofilms. *Appl Environ Microbiol* **70:** 6188–6196.

Xavier, J.B., Picioreanu, C., and van Loosdrecht, M.C.M. (2005) A general description of detachment for multidimensional modeling of biofilms. *Biotechnol Bioeng* **91:** 651–669.

Yang, X., Beyenal, H., Harkin, G., and Lewandowski, Z. (2000) Quantifying biofilm structure using image analysis. *J Microbiol Methods* **39:** 109–119.

Supplementary material

The following supplementary material is available for this article online:

Table S1. Displacement table for individual clusters showing centroid coordinates, and calculated displacement distances, angles and velocities.

Table S2. Accumulation and displacement analysis for the three pockets of cells within the large cyan cluster shown in Fig. 1.

This material is available as part of the online article from http://www.blackwell-synergy.com

Please note: Blackwell Publishing is not responsible for the content or functionality of any supplementary materials supplied by the authors. Any queries (other than missing material) should be directed to the corresponding author for the article.

© 2008 The Authors
Journal compilation © 2008 Society for Applied Microbiology and Blackwell Publishing Ltd,